Taming the Dynamical Sign Problem in Real-Time Evolution of Quantum Many-Body Problems

Guy Cohen,[1,2] Emanuel Gull,[3] David R. Reichman,[1] and Andrew J. Millis[2]
[1]Department of Chemistry, Columbia University, New York, New York 10027, USA
[2]Department of Physics, Columbia University, New York, New York 10027, USA
[3]Department of Physics, University of Michigan, Ann Arbor, Michigan 48109, USA
(Received 12 October 2015; published 23 December 2015)

Current nonequilibrium Monte Carlo methods suffer from a dynamical sign problem that makes simulating real-time dynamics for long times exponentially hard. We propose a new "inchworm algorithm," based on iteratively reusing information obtained in previous steps to extend the propagation to longer times. The algorithm largely overcomes the dynamical sign problem, changing the scaling from exponential to quadratic. We use the method to solve the Anderson impurity model in the Kondo and mixed valence regimes, obtaining results both for quenches and for spin dynamics in the presence of an oscillatory magnetic field.

DOI: 10.1103/PhysRevLett.115.266802 PACS numbers: 73.63.Kv, 72.10.Fk, 73.21.La, 85.65.+h

The nonequilibrium physics of quantum many-body systems is a central topic of current research [1]. Experimentally, the application of strong currents through quantum dots [2], molecular junctions [3] and extended systems, the optical excitation of high densities of carriers above band gaps of Mott insulators [4], and high amplitude terahertz coupling to phonon modes [5] have revealed exciting new physics. In cold atoms sudden parameter quenches have also been studied [6–8]. While remarkable experimental progress has been made, theory faces a crucial limitation: numerical calculations of time-dependent and nonequilibrium problems suffer from an exponential scaling of computational cost with simulation time. In different formulations the problem manifests in different ways: as a mixing of low- and high-energy states as time progresses in truncated wave function methods like time-dependent numerical renormalization group (NRG) [9] or density matrix renormalization group (DMRG) [10–12], as an exponential number of operators needed to reach a given accuracy in the hierarchical equations of motion [13–17], or as a "dynamical" sign problem in nonequilibrium quantum Monte Carlo (QMC) methods [18–21]. In practice, the exponential scaling in known numerically exact methods has prevented accurate numerical calculations of the long-time behavior of nonequilibrium correlated systems.

Diagrammatic QMC methods, which provide numerically exact solutions by stochastically sampling a perturbation series, have been particularly fruitful in elucidating the physics in equilibrium, where the problem can be formulated in imaginary time [22–30]. Straightforward extension of these methods to nonequilibrium [18–21] requires estimation of integrals that contain combinations of oscillating exponentials $\exp(iHt)$; as the integrals extend over longer time ranges, numerical difficulties limit the times accessible in the strong coupling regime to the order of the typical tunneling time scale. Longer times can be reached by sampling corrections to semianalytic theories such as the none- and one-crossing approximations (NCA [31,32] and OCA [33–35]), by explicit summation over Keldysh indices followed by a continuation on the complex plane [36], and with memory function techniques [37–40]. Nevertheless, all of these methods encounter an exponential wall as time is increased, limiting their applicability to relatively short time dynamics or to the weak correlation regime.

In this Letter we present an algorithm whose computational cost scales *quadratically* rather than exponentially with time, allowing controlled numerical access to the long-time behavior of strongly correlated quantum systems. The algorithm is based on iteratively reusing information from shorter time propagation to obtain results for longer times, is generally applicable to any diagrammatic method, and has a straightforward interpretation in terms of self-consistent skeleton expansions. The method presented here deals only with the dynamical sign problem, not with the intrinsic fermionic one, which limits access to certain systems even in equilibrium. However, a spatial inchworm algorithm (as opposed to the temporal one presented here) might make headway against that problem. We implement the algorithm for the Anderson impurity model (AIM) in the strongly correlated Kondo and mixed-valence regimes, and show that it captures the long-time spin dynamics after a quantum quench and in the presence of an oscillating magnetic field. While the results presented here pertain to impurity models, the algorithm itself should prove useful beyond this context in the more general quantum many-body setting.

The crucial object in the algorithm is the Keldysh-contour propagator $G_{\alpha\alpha'}(t_f, t_i)$ giving the transition amplitude between state α at initial contour time t_i and state α' at

final contour time t_f in the presence of a Hamiltonian $H = H_0(t) + V(t)$:

$$G_{\alpha\alpha'}(t_f, t_i) \equiv \langle \alpha | \mathrm{Tr}_{\mathcal{B}} \left\{ e^{i \int_{t_i}^{t_f} d\tilde{t} H_0(\tilde{t}) + V(\tilde{t})} \right\} | \alpha' \rangle. \quad (1)$$

Reference [35] discusses such propagators and their relationship to observables. H_0 is assumed to be an exactly solvable Hamiltonian, and one studies G by an expansion in iV, as illustrated for an impurity model expansion (where all propagators can be collapsed onto a single line) in Fig. 1. Figure 1(a) represents a bare expansion, where G (thick line) is evaluated by summing all possible interaction lines in terms of a bare propagator (thin line). Figure 1(b) represents a particular bold-line expansion, where an approximate propagator (represented by a medium or "bold" line) containing a subset of the interactions is evaluated semianalytically, and all corrections are summed in terms of the bold propagator. Importantly, G is contour causal: in the expansion only vertices $V(\tilde{t})$ for which $t_i < \tilde{t} < t_f$ occur. The factors of iV cause a dynamical sign problem, and in the approaches used to date, the expansion order (number of iV insertions) is proportional to the final time simulated. Our algorithm avoids this by using a kind of skeleton expansion: it exploits the contour causal nature of G to construct an exact propagator for longer times in terms of an exact propagator for shorter times, iteratively increasing the time up to which propagators are known. We observe that the sign problem does not worsen as a function of time, resulting in quadratic algorithmic scaling overall.

The algorithm, which we illustrate in Fig. 1(c), begins from the assumption that $G_{\alpha\alpha'}(t_1, t_2)$ is known for all values

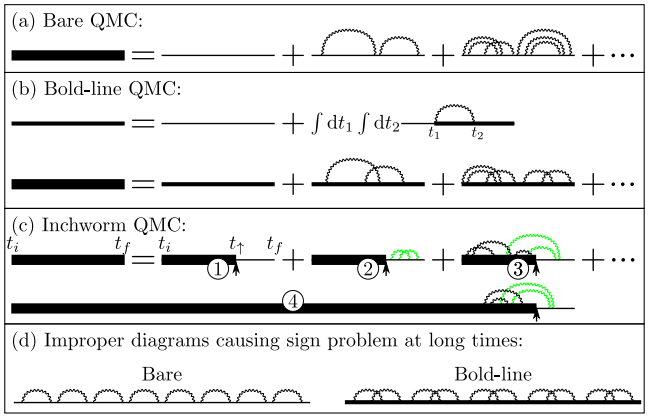

FIG. 1 (color online). Comparison of diagrams sampled in previous approaches [bare expansion (a) [18,19] and bold expansion (b) [31,32]] to diagrams sampled in new approach (c), and diagrams leading to dynamical sign problem in previous methods (d). Thick lines: full propagators. Thin lines: bare propagators. Medium ("bold") lines: propagators resulting from analytical resummation of subset of diagrams (here, NCA). Wiggly lines: hybridization lines. Arrows indicate $t_\uparrow$.

of t_1 and t_2 less than a designated time $t_\uparrow$. We now consider the terms appearing in a computation of $G_{\alpha\alpha'}(t_f, t_i)$ for $t_f > t_\uparrow$. If no interactions occur or all interactions occur before $t_\uparrow$, the term can be subsumed into the (known) propagation from t_i to $t_\uparrow$, followed by a bare propagation from $t_\uparrow$ to t_f, as illustrated in diagram (1) of Fig. 1(c). If interactions occur after $t_\uparrow$ but no interaction lines connect times after $t_\uparrow$ to times before $t_\uparrow$, the propagation to $t_\uparrow$ is captured by the known $G_{\alpha\alpha'}(t_\uparrow, t_i)$, with the usual perturbation in V required to capture propagation in the interval $t_\uparrow \to t_f$ [see diagram (2)]. Finally, terms with interaction lines spanning $t_\uparrow$ can be subsumed into diagrams with exact propagators before $t_\uparrow$ and bare propagators after $t_\uparrow$ by absorbing any interaction line that is not connected to a line reaching past $t_\uparrow$ in the exact propagator [diagram (3)].

By summing these three classes of diagrams [(1), (2), (3)] we count each bare diagram exactly once, producing a formally exact solution for the propagator $G_{\alpha\alpha'}(t_1, t_2)$. The procedure crucially relies on the contour-time causality of the propagator: $G_{\alpha\alpha'}(t_1, t_2)$ contains all possible diagrams with interaction lines between t_2 and t_1 but no interaction lines outside of this interval.

The main advantage is that improper repetitions of simple inclusions [see Fig. 1(d)] are absorbed in the propagator for $t < t_\uparrow$ and only need to be sampled for $t > t_\uparrow$. The number of these diagrams grows exponentially as a function of propagation time, causing the dynamical sign problem: consider that the number of possible locations for inclusions increases roughly linearly with the length of the propagation time. Since each individual inclusion might be removed, this generates an exponential number of possible diagrams. $t_\uparrow$ is a free parameter: as $t_\uparrow$ is lowered to t_i, the procedure reverts to the standard bare expansion in V [see Fig. 1(a)]. As $t_\uparrow$ is increased towards t_f, fewer diagrams are sampled, but the exact propagator has to be known for longer times.

The possibility of obtaining propagators based on corrections to propagators for smaller times suggests a numerical algorithm: starting from the knowledge of the exact propagators within a short time interval (t_i, t_f^n) with $t_f^n = t_i + n\Delta t$, e.g., as obtained from a bare Monte Carlo simulation, we calculate propagators for the longer interval $(t_i, t_f^n + \Delta t) = (t_i, t_f^{n+1})$ by setting $t_\uparrow = t_f^n$ and sampling again the three classes of diagrams described in Fig. 1(c). The process is iteratively repeated, gradually increasing the interval on which propagators are known by "inching" along the Keldysh contour. These successive small steps, which gradually increase t_f, have led us to term this procedure the inchworm algorithm. We note in passing that at the limit $\Delta t \to 0$ the quantity summed in the expansion introduced above becomes a product of the proper propagator self-energy and the full propagator.

Since $G_{\alpha\alpha'}(t_f, t_i)$ has two time arguments, propagation must be carried out in both temporal directions. To reach a final time t at a discretization of Δt requires $\frac{1}{4}(t/\Delta t)^2$

interdependent simulations when causality and time-reversal symmetry are taken into account, resulting in an algorithm that scales at least quadratically. To control the complexity of the computation, it is also useful to limit the maximum order of diagrams to be sampled and then verify convergence with respect to increasing the diagram order [25,32]. It can be shown that inchworm QMC calculations truncated at a given order corresponds as $\Delta t \to 0$ to a self-consistent skeleton expansion with the self-energy truncated to the same order (since the included terms are given by all proper inclusions up to the respective order, in terms of propagators containing the same). Based on experience from these methods [41] we may therefore expect that most contributions at long times will include interaction lines at only a limited, time-independent range from the final time, as illustrated in diagram (4) of Fig. 1(c).

We illustrate the inchworm scheme with the example of an AIM with a time- and spin-dependent local field:

$$H(t) = \sum_{\sigma\in\{\uparrow,\downarrow\}} \varepsilon_\sigma(t) d_\sigma^\dagger d_\sigma + U n_\uparrow n_\downarrow + \sum_{\sigma k} \varepsilon_{\sigma k} a_{\sigma k}^\dagger a_{\sigma k} + \sum_{a\sigma k} (V_{\sigma k} a_{\sigma k}^\dagger d_\sigma + \text{H.c.}). \quad (2)$$

ε_σ are on-site level energies, $\sigma \in \{1,-1\}$ a spin index, and U is the on-site Coulomb interaction. $\varepsilon_{\sigma k}$ and $V_{\sigma k}$ are fully defined by the dot-bath coupling, which we set to $\Gamma(\omega) = 2\pi\sum_k V_{\sigma k}^* V_{\sigma k}\delta(\omega-\varepsilon_k) = \Gamma/[(1+e^{\nu(\omega-\Omega_c)})(1+e^{-\nu(\omega+\Omega_c)})]$, with $\nu = 10/\Gamma$ and $\Omega_C = 10\Gamma$. We simulate a coupling quench, i.e., the dynamics of a dot initially decoupled from the bath, with the coupling turned on instantaneously at time zero. We use the hybridization expansion, where the interaction Hamiltonian V is taken to be the final term in Eq. (2) (a detailed review is found in Ref. [28]).

In the top panel of Fig. 2 we show the time evolution of the four populations (diagonal density matrix elements) after a quench, as described by the bare hybridization expansion for times $t \lesssim 1.5$ (light lines) and by our inchworm algorithm (dark lines). The system, initially in state $|\uparrow\rangle$, slowly relaxes to a configuration in which $\uparrow$ and $\downarrow$ are degenerate. We observe that the two numerically exact algorithms agree within errors, but for $t \gtrsim 1$, bare QMC results become noisy.

The bottom panel of Fig. 2 shows that the bare error increases exponentially in time (for the constant simulation time per point used here). This is a direct consequence of the dynamical sign problem. In contrast, the inchworm error plateaus, allowing access to significantly longer times. To account for the propagation of errors from short times to longer times, the inchworm error estimate has been obtained from the standard deviations between independent runs with uncorrelated statistical errors. The plateau of the noise implies that the average sign stays constant as a function of time, and that there is no observable error amplification due to repeated use of propagators from earlier times. We have verified that significantly larger errors than those used here do not result in a bias (not shown). Of course, if the noise is allowed to grow dominant the calculation fails (also not shown).

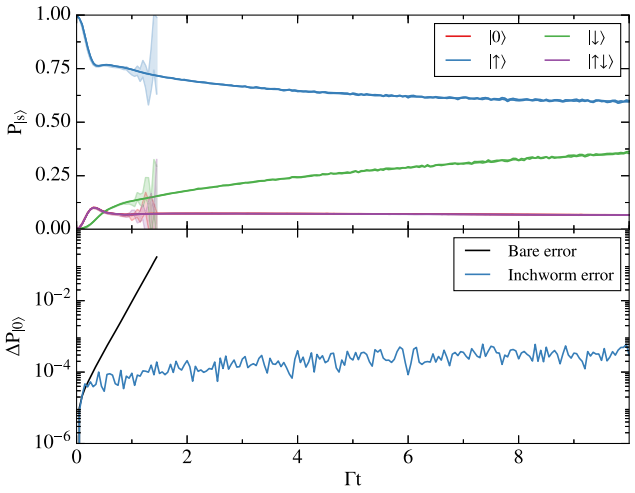

FIG. 2 (color online). Top: AIM population dynamics in the Kondo regime following a coupling quench from a fully magnetized state at $U = -2\varepsilon = 8\Gamma$ and inverse temperature $\beta\Gamma = 50$. The bare hybridization expansion result [Fig. 1(a)] is shown for times $\Gamma t < 1.5$, along with the inchworm result [Fig. 1(c)] up to $\Gamma t = 10$ (the maximum order is limited to 3, at which convergence occurs). Bottom: Error estimate of data in upper panel showing exponential increase of the error as a function of time due to the dynamical sign problem in the bare method, and roughly constant error in the inchworm method.

To assess convergence with expansion order, we plot the magnetization $P_{|\uparrow\rangle} - P_{|\downarrow\rangle}$ as a function of time in Fig. 3.

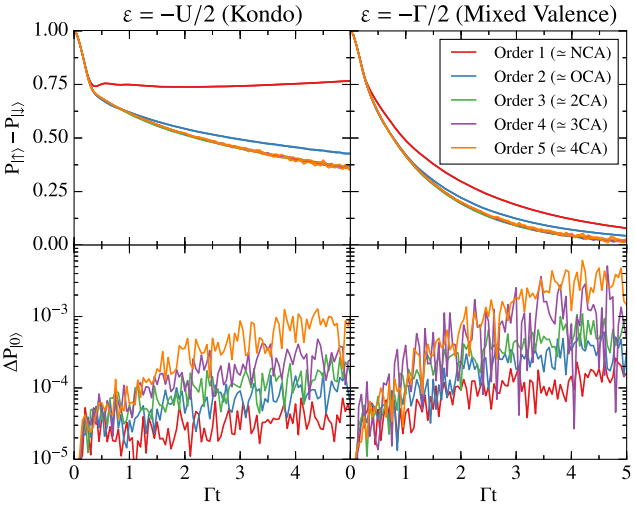

FIG. 3 (color online). Top: Population as a function of time after a coupling quench at $U = 8\Gamma$ and inverse temperature $\beta\Gamma = 50$, computed for a system in the Kondo regime (left-hand panels) and in the mixed valence regime (right-hand panels). Different traces show the convergence as a function of inchworm expansion order. Bottom: Error estimate of the populations for different inchworm expansion orders as a function of time.

The left-hand panel shows parameters in the Kondo regime $\varepsilon_\sigma = -U/2$, the right-hand panel shows parameters in the mixed valence regime $\varepsilon_\sigma = -\Gamma/2$. Results of the inchworm method are exact only at infinite expansion order. If the maximum expansion order is artificially restricted to 1, the relaxation to steady state is slow (right-hand panel) or even absent (left-hand panel). As the maximum order is gradually increased, the relaxation time scales shorten and (for these parameters) converge at an expansion order of ~3–4. In the limit $\Delta t \to 0$ (we used a small but nonzero $\Delta t = 0.05/\Gamma$), the diagrams enumerated by the inchworm algorithm correspond to the NCA diagrams for order 1, the OCA diagrams for order 2, the two-crossing diagrams for order 3, etc. Figure 3, therefore, shows that at least a two-crossing approximation is required to correctly capture the real-time evolution of this system.

The error analysis (bottom panels of Fig. 3) reveals that the error for each order first increases, then converges to a constant, thereby overcoming the exponential scaling commonly associated with a sign problem. The error increases with order, since the sampling space grows larger and the calculations are performed at fixed computational cost. However, because the error rises by an approximately constant factor between any two orders, it may be eliminated by a small constant increase in computer time (a factor of ~3 in this case). This graceful scaling, along with the rapid convergence to the exact result, establishes the algorithm's numerical exactness.

While the same results could be obtained by increasing the order of a semianalytical skeleton expansion (e.g., improving the level of approximation from noncrossing to one crossing to two crossing, etc.), the computational expense typically increases very rapidly [the cost of each added crossing in an n-crossing approximation is $\sim(t/\Delta t)^2$]. In practice, to our knowledge, nonequilibrium calculations even at the two-crossing level have been performed only to relatively short time [41], and higher-order calculations have not been carried out. Figure 3 shows that the inchworm algorithm can access the three- and four-crossing approximations.

Figure 4 displays the time dependence of the probability that the dot is empty or doubly occupied (reflecting charge dynamics) and the magnetization, starting from either an unmagnetized initial state (top panels) or a fully magnetized initial state (bottom panels) and computed in the presence of an oscillating magnetic field $(\varepsilon_\uparrow - \epsilon_\downarrow)(t) = 2h\sin(\omega t)$. The response to oscillating fields has been studied in the context of currents induced by oscillating voltages [42,43]. Current relaxation is rather fast even in the Kondo regime [32], so the numerical problems are less severe, but even in this case the equation of motion methodology used in the more recent studies can have convergence issues in the Kondo regime [16,17]. Here, we focus on the more challenging issue of the spin dynamics. Three regimes are compared: the noninteracting

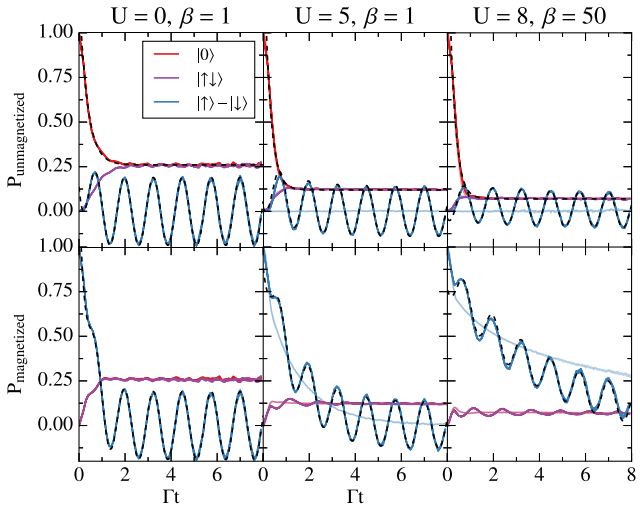

FIG. 4 (color online). AIM population and magnetization dynamics at interaction strengths and temperatures shown, in the presence of a time-dependent magnetic field $h(t)=2\Gamma\sin(\omega t)$, with $\omega = 5\Gamma$. Dot is initially in the empty state $|0\rangle$ (top row) or in the fully magnetized state $|\uparrow\rangle$ (bottom). Lighter curves show time evolution for $h = 0$ with otherwise identical parameters. Dashed black curves show fits to $f(t) = A + Be^{-\gamma t} + C\sin(\omega_0 t + \phi)$. In units where $\Gamma = 1$, the charge relaxation rates (γ for $|0\rangle$, $|\uparrow\downarrow\rangle$) are $\gamma_c = 2.83$, 3.8, and 4.0 for $(U,\beta) = (0,1)$, (5.0,1), and (8.0,50), respectively. The spin relaxation rates in the presence of the field are $\gamma_s = 3.3$, 0.81, and 0.25 (dot initially empty) and 2.4, 0.81, and 0.25 (dot initially fully magnetized). The spin relaxation rates for $h = 0$ are 0.68 for $U = 5, \beta = 1$, and 0.11 for $U = 8, \beta = 50$. The final amplitudes C are 0.19, 0.13, and 0.1. $\phi = -2$ in all cases.

case (left-hand panel), the edge of the Kondo regime (center panel), and deeper in the Kondo regime (right-hand panel). As U is increased and the temperature decreased, the charge relaxation time is shortened while the spin relaxation time lengthens dramatically. We quantify the effects by fitting the data to the simple phenomenological form $f(t) = A + Be^{-\gamma t} + C\sin(\omega_0 t + \phi)$. Fits are seen to be extremely good and reveal a more than factor of 10 increase in the spin lifetime and 50% decrease in the charge lifetime as the Kondo regime is entered, as well as an interesting dependence of the spin relaxation time on the strength of the oscillating field. A more detailed study of the spin dynamics and its dependence on the driving field will be presented elsewhere.

In conclusion, we have presented a QMC method for real-time propagation which we have termed the inchworm algorithm, as it is based on gradually inching along the Keldysh contour. The algorithm takes advantage of previously computed propagation information by reusing it when extending the propagation to longer times. This technique could be applied to any quantum many-body system, but its general usefulness still requires investigation. We have implemented the algorithm for the AIM in the hybridization expansion, where we were able to access

slow spin dynamics in the strongly correlated Kondo regime and observe its response to an oscillating magnetic field. Our method suppresses the dynamical sign problem to such a degree that the polynomially scaling part of the algorithm becomes dominant. We also showed how high-order skeleton expansions are accessible by truncating the expansion, at a scaling which is quadratic at any order rather than being governed by a power law with the power proportional to the order.

The authors would like to thank Andrey Antipov and Yevgeny Bar Lev for helpful comments and discussions. A. J. M. and G. C. acknowledge support from the Department of Energy under Grant No. DE-SC0012375. E. G. acknowledges support by DOE ER 46932. D. R. R. acknowledges support by NSF CHF 1464802.

[1] J. Eisert, M. Friesdorf, and C. Gogolin, Nat. Phys. **11**, 124 (2015).
[2] W. G. van der Wiel, S. De Franceschi, J. M. Elzerman, T. Fujisawa, S. Tarucha, and L. P. Kouwenhoven, Rev. Mod. Phys. **75**, 1 (2002).
[3] N. A. Zimbovskaya and M. R. Pederson, Phys. Rep. **509**, 1 (2011).
[4] A. Dienst, E. Casandruc, D. Fausti, L. Zhang, M. Eckstein, M. Hoffmann, V. Khanna, N. Dean, M. Gensch, S. Winnerl, W. Seidel, S. Pyon, T. Takayama, H. Takagi, and A. Cavalleri, Nat. Mater. **12**, 535 (2013).
[5] M. Liu, H. Y. Hwang, H. Tao, A. C. Strikwerda, K. Fan, G. R. Keiser, A. J. Sternbach, K. G. West, S. Kittiwatanakul, J. Lu, S. A. Wolf, F. G. Omenetto, X. Zhang, K. A. Nelson, and R. D. Averitt, Nature (London) **487**, 345 (2012).
[6] L. E. Sadler, J. M. Higbie, S. R. Leslie, M. Vengalattore, and D. M. Stamper-Kurn, Nature (London) **443**, 312 (2006).
[7] D. Chen, M. White, C. Borries, and B. DeMarco, Phys. Rev. Lett. **106**, 235304 (2011).
[8] M. Gring, M. Kuhnert, T. Langen, T. Kitagawa, B. Rauer, M. Schreitl, I. Mazets, D. A. Smith, E. Demler, and J. Schmiedmayer, Science **337**, 1318 (2012).
[9] F. B. Anders and A. Schiller, Phys. Rev. Lett. **95**, 196801 (2005).
[10] S. R. White and A. E. Feiguin, Phys. Rev. Lett. **93**, 076401 (2004).
[11] G. Vidal, Phys. Rev. Lett. **93**, 040502 (2004).
[12] A. J. Daley, C. Kollath, U. Schollwöck, and G. Vidal, J. Stat. Mech. (2004) P04005.
[13] Y. Tanimura, J. Phys. Soc. Jpn. **75**, 082001 (2006).
[14] S. Welack, M. Schreiber, and U. Kleinekathöfer, J. Chem. Phys. **124**, 044712 (2006).
[15] J. Jin, X. Zheng, and Y. Yan, J. Chem. Phys. **128**, 234703 (2008).
[16] R. Härtle, G. Cohen, D. R. Reichman, and A. J. Millis, Phys. Rev. B **88**, 235426 (2013).
[17] R. Härtle, G. Cohen, D. R. Reichman, and A. J. Millis, Phys. Rev. B **92**, 085430 (2015).
[18] L. Mühlbacher and E. Rabani, Phys. Rev. Lett. **100**, 176403 (2008).
[19] P. Werner, T. Oka, and A. J. Millis, Phys. Rev. B **79**, 035320 (2009).
[20] M. Schiró, Phys. Rev. B **81**, 085126 (2010).
[21] A. E. Antipov, Q. Dong, and E. Gull, arXiv:1508.06633.
[22] N. V. Prokof'ev, B. V. Svistunov, and I. S. Tupitsyn, Phys. Lett. A **238**, 253 (1998).
[23] A. N. Rubtsov, V. V. Savkin, and A. I. Lichtenstein, Phys. Rev. B **72**, 035122 (2005).
[24] P. Werner, A. Comanac, L. de' Medici, M. Troyer, and A. J. Millis, Phys. Rev. Lett. **97**, 076405 (2006).
[25] N. Prokof'ev and B. Svistunov, Phys. Rev. Lett. **99**, 250201 (2007).
[26] N. V. Prokof'ev and B. V. Svistunov, Phys. Rev. B **77**, 125101 (2008).
[27] E. Gull, P. Werner, O. Parcollet, and M. Troyer, Europhys. Lett. **82**, 57003 (2008).
[28] E. Gull, A. J. Millis, A. I. Lichtenstein, A. N. Rubtsov, M. Troyer, and P. Werner, Rev. Mod. Phys. **83**, 349 (2011).
[29] P. Sémon and A.-M. S. Tremblay, Phys. Rev. B **85**, 201101 (2012).
[30] H. Shinaoka, Y. Nomura, S. Biermann, M. Troyer, and P. Werner, Phys. Rev. B **92**, 195126 (2015).
[31] E. Gull, D. R. Reichman, and A. J. Millis, Phys. Rev. B **82**, 075109 (2010).
[32] E. Gull, D. R. Reichman, and A. J. Millis, Phys. Rev. B **84**, 085134 (2011).
[33] G. Cohen, E. Gull, D. R. Reichman, A. J. Millis, and E. Rabani, Phys. Rev. B **87**, 195108 (2013).
[34] G. Cohen, E. Gull, D. R. Reichman, and A. J. Millis, Phys. Rev. Lett. **112**, 146802 (2014).
[35] G. Cohen, D. R. Reichman, A. J. Millis, and E. Gull, Phys. Rev. B **89**, 115139 (2014).
[36] R. E. V. Profumo, C. Groth, L. Messio, O. Parcollet, and X. Waintal, Phys. Rev. B **91**, 245154 (2015).
[37] G. Cohen and E. Rabani, Phys. Rev. B **84**, 075150 (2011).
[38] G. Cohen, E. Y. Wilner, and E. Rabani, New J. Phys. **15**, 073018 (2013).
[39] E. Y. Wilner, H. Wang, G. Cohen, M. Thoss, and E. Rabani, Phys. Rev. B **88**, 045137 (2013).
[40] E. Y. Wilner, H. Wang, M. Thoss, and E. Rabani, Phys. Rev. B **89**, 205129 (2014).
[41] M. Eckstein and P. Werner, Phys. Rev. B **82**, 115115 (2010).
[42] P. Nordlander, N. S. Wingreen, Y. Meir, and D. C. Langreth, Phys. Rev. B **61**, 2146 (2000).
[43] X. Zheng, Y. J. Yan, and M. Di Ventra, Phys. Rev. Lett. **111**, 086601 (2013).